

Multipath Curved Planar Reformation of the Peripheral Arterial Tree in CT Angiography¹

Justus E. Roos, MD
 Dominik Fleischmann, MD
 Arnold Koechl, MD
 Tejas Rakshe, MS
 Matus Straka, MS
 Alessandro Napoli, MD
 Armin Kanitsar, PhD
 Milos Sramek, PhD
 Eduard Groeller, PhD

The study was approved by the institutional review board, and informed consent was obtained. The purpose of the study was to prospectively quantify the angular visibility range, determine the existence of orthogonal viewing pairs, and characterize the conditions that cause artifacts in multipath curved planar reformations (MPCPRs) of the peripheral arterial tree in 10 patients (eight men and two women; mean age, 69 years; range, 54–80 years) with peripheral arterial occlusive disease. Percentage of segments with the maximal possible visibility score of 1 was significantly greater (odds ratio, 1.42; $P < .001$) for MPCPRs than for maximum intensity projections. One or more orthogonal viewing pairs were identified for all above-knee arterial segments, and artifactual vessel distortion was observed when the vessel axis approached a horizontal course in MPCPRs.

© RSNA, 2007

Supplemental material:
<http://radiology.rsna.org/cgi/content/full/2441060976/DC1>

¹ From the Department of Radiology, Stanford University Medical Center, 300 Pasteur Dr, Room S-072, Stanford, CA 94305-5105 (J.E.R., D.F., T.R., A.N.); Department of Angiography and Interventional Radiology, Medical University of Vienna, Vienna General Hospital, Vienna, Austria (D.F., A. Koechl); Commission for Scientific Visualization, Austrian Academy of Sciences, Vienna, Austria (M. Straka, M. Sramek); and Institute of Computer Graphics and Algorithms, Vienna University of Technology, Vienna, Austria (A. Kanitsar, E.G.). Received June 6, 2006; revision requested August 8; revision received August 25; accepted September 27; final version accepted November 1. Supported by grants P-15217 and L291-N04 from the Austrian Science Fund. J.E.R. supported by grant PBBEB 106796 from the Swiss National Science Foundation. **Address correspondence to D.F.** (e-mail: d.fleischmann@stanford.edu).

© RSNA, 2007

Computed tomographic (CT) angiography of the peripheral arteries has evolved into an accurate and cost-effective noninvasive imaging technique in patients with peripheral arterial occlusive disease (PAOD) (1–3). Although CT angiographic data acquisition is straightforward, effective visualization and communication of the complex multifocal manifestations of PAOD remain a major challenge (4). Maximum intensity projection (MIP) and volume rendering provide excellent angiographiclike images of the peripheral arteries; however, both techniques do not exhibit the arterial lumen when vessel wall calcifications or stents are present. Interpretation of CT angiograms of the peripheral arteries therefore mandates the review of two-dimensional cross-sectional images.

Transverse CT source images (5–9), coronal and sagittal multiplanar reformations (5), double-oblique multiplanar reformations perpendicular to the vessel centerline (10), and curved planar reformations that follow an arterial centerline (8,11,12) all serve this purpose. Curved planar reformations provide an intuitive longitudinal cross-sectional view of diseased arterial segments; however, standard single-path curved planar reformations (SPCPRs) can only display one arterial segment at a time (12–14) and are, thus, not truly comprehensive for visualization of the entire peripheral arterial tree. Another limita-

tion of SPCPRs is limited spatial perception. Without anatomic landmarks—such as vessel bifurcations—in the reconstructed image plane, the viewer may not be able to identify the vessel of interest.

A proposed technical solution to this problem is the generation of multipath curved planar reformations (MPCPRs) (15). An MPCPR image provides a simultaneous display of multiple longitudinal cross sections through the centerlines of the entire peripheral arterial tree and restores spatial perception by displaying the familiar branching pattern (Fig 1).

This obvious potential advantage of MPCPRs for more comprehensive visualization of the diseased peripheral arterial tree has to be weighed against its limitations, such as viewing angle-dependent superimposition, obscuration of arterial branches, and specific artifacts. Thus, the purpose of our study was to prospectively quantify the angular visibility range, determine the existence of orthogonal viewing pairs, and characterize the conditions that cause artifacts in MPCPRs of the peripheral arterial tree in patients with PAOD.

Materials and Methods

Patients and Image Acquisition Parameters

Ten patients (eight men and two women; mean age, 69 years; range, 54–80 years) with PAOD were invited to participate in this prospective study. All patients were referred from the Department of Vascular Surgery, Medical University of Vienna, Vienna General Hospital, Vienna, Austria, for angiographic evaluation of PAOD between January and March 2001, before diagnostic DSA was replaced with CT an-

giography and magnetic resonance angiography in the Department of Angiography and Interventional Radiology at Medical University of Vienna. The study protocol specifically aimed at the collection of data sets for the prospective evaluation of new visualization tools and was approved by the ethics committee of Medical University of Vienna. Written informed consent was obtained from all individuals after they were given a thorough explanation of the study purpose and the involved risks, such as additional radiation exposure during CT angiography.

CT angiograms were obtained with a four-channel multi-detector row CT scanner (Somatom Plus 4 Volume Zoom; Siemens Medical Systems, Erlangen, Germany) during intravenous injection of 95–130 mL of iopamidol (Iopamirol; Bracco, Milan, Italy) that contained 300 mg of iodine per milliliter. Scanning parameters were 120 kVp, 130 mAs, a detector configuration of four detector rows with a section thickness of 2.5 mm, and a pitch of 1.5. Transverse 3-mm-thick sections

Advances in Knowledge

- Multipath curved planar reformation (MPCPR) allows the simultaneous display of longitudinal cross sections through all major conducting arteries of the lower extremities at arbitrary viewing angles.
- MPCPR displays the peripheral arterial tree over a significantly greater viewing range than does maximum intensity projection (MIP).
- MPCPR causes specific predictable artifacts with certain conditions, such as vessels that run parallel to the horizontal axis.

Implication for Clinical Care

- Although MPCPRs cannot completely replace MIPs or standard single-path curved planar reformations, they may facilitate the visualization of aortoiliac and femoropopliteal arteries in patients with peripheral arterial occlusive disease.

Published online before print
10.1148/radiol.2441060976

Radiology 2007; 244:281–290

Abbreviations:

ATA = anterior tibial artery
CFA = common femoral artery
CIA = common iliac artery
DICOM = Digital Imaging and Communications in Medicine
DSA = digital subtraction angiography
EIA = external iliac artery
MPCPR = multipath curved planar reformation
MIP = maximum intensity projection
OR = odds ratio
PAOD = peripheral arterial occlusive disease
SPCPR = single-path curved planar reformation
SFA = superficial femoral artery
TPT = tibioperoneal trunk

Author contributions:

Guarantors of integrity of entire study, J.E.R., D.F.; study concepts/study design or data acquisition or data analysis/interpretation, all authors; manuscript drafting or manuscript revision for important intellectual content, all authors; manuscript final version approval, all authors; literature research, J.E.R., D.F., A.N., M. Sramek, E.G.; clinical studies, D.F., A. Koechl; experimental studies, M. Sramek; statistical analysis, J.E.R., D.F., A.N.; and manuscript editing, J.E.R., D.F., T.R., A.N., A. Kanitsar, M. Sramek, E.G.

Authors stated no financial relationship to disclose.

were reconstructed at 1-mm intervals. All patients underwent complete intraarterial DSA within 1 week after CT angiography. Angiograms were obtained by faculty radiologists or supervised trainees at the Department of Angiography and Interventional Radiology, Medical University of Vienna. DSA images were stored in the local picture archiving and communication system. The rationale for recording DSA data was to provide a potential reference standard if different postprocessing techniques would result in an unexpected display of peripheral arteries.

Semiautomated Extraction of the Arterial Centerline Tree

CT images were networked to a research computer workstation, converted into a compressed three-dimensional file format (16), and stored in a local database. One radiologist (D.F.), with 7 years of experience in CT angiography, used a semiautomated vessel tracking and centering algorithm (17) to extract the arterial centerline trees between a starting point in the abdominal aorta and six end points located in the bilateral dorsalis pedis, the common plantar arteries, and the most distal portions of the peroneal arteries (Fig 1). User interaction for vessel tree extraction took between 5 and 25 minutes. The result of this vessel extraction step was stored to a file (tree file) for later use.

Generation of MPCPRs and SPCPRs

The generation of MPCPRs and SPCPRs is fully automated. Each patient's compressed image data and the corresponding postprocessing information (tree file) are loaded together to generate 21 MPCPR images over a viewing range of 180° (from left lateral [−90°] through anteroposterior [0°] to right lateral [+90°] viewing angles) in 9° intervals. SPCPRs are created over the same 180° viewing range (in 18° intervals) through each of a patient's six (three left and three right) aortocrural centerlines. All images were saved in Digital Imaging and Communications in Medicine (DICOM) format to preserve the original CT resolution and attenuation information and were grouped into DICOM series

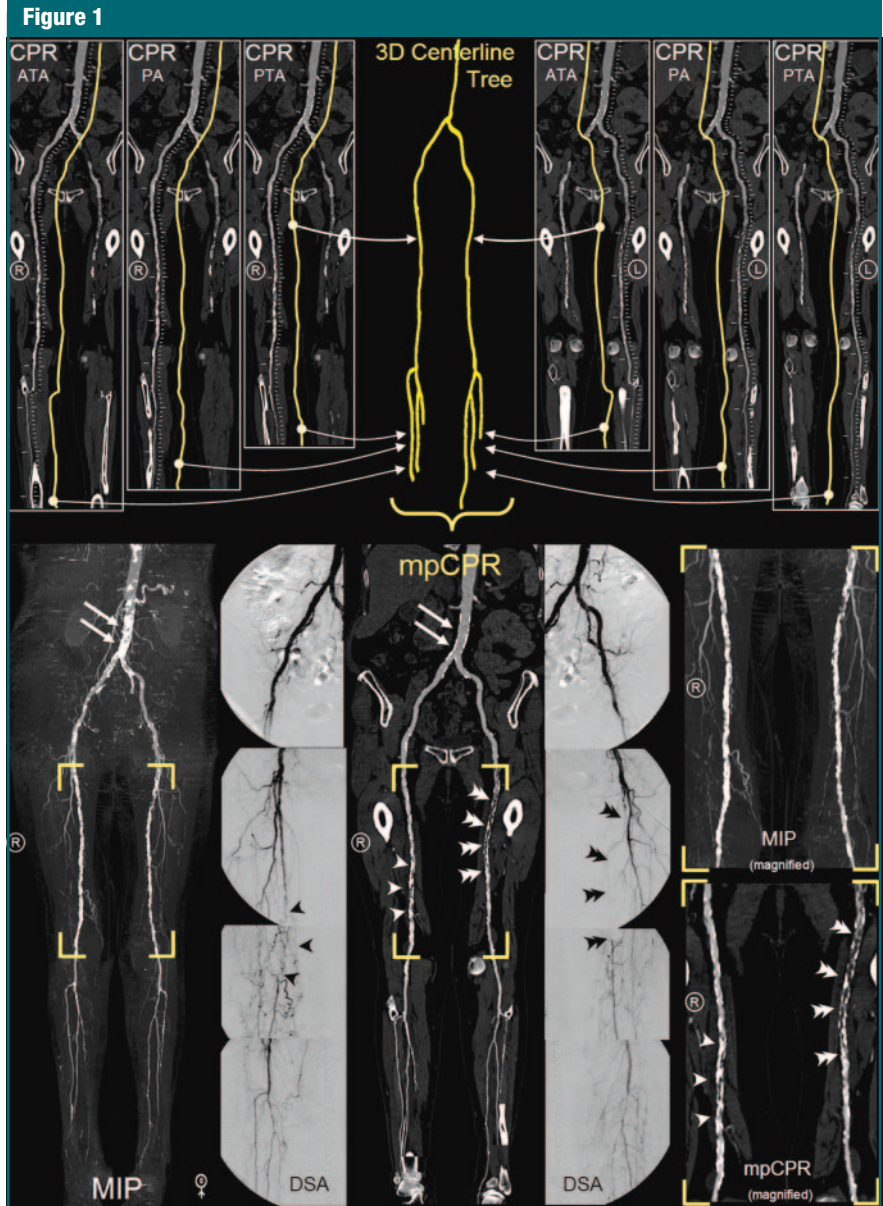


Figure 1: Schematic of MPCPR. Generation of MPCPR of the peripheral arterial tree in a 72-year-old woman with bilateral calf claudication, in comparison with SPCPR (CPR), digital subtraction angiographic (DSA), and MIP images. Top: After semiautomated extraction of the vascular centerlines through all major conducting vessels (three-dimensional [3D] centerline tree), multiple SPCPRs through each centerline branch can be created from the aorta through the bilateral anterior tibial artery (ATA), posterior tibial artery (PTA), and peroneal artery (PA). Yellow lines drawn parallel to the arterial branches in panels highlight the respective centerline path used for curved planar reformation generation. Note that SPCPR images can show only one vessel at a time and that six images are required for complete visualization in the anteroposterior viewing direction. Bottom: With MPCPR, information from the entire three-dimensional centerline tree is used to assemble a composite image that simultaneously displays longitudinal cross sections through all peripheral arteries in a single anteroposterior view. Although MIP does not allow the assessment of the arterial flow lumens in the aorta (arrows) and in the right (arrowheads) and left (double arrowheads) superficial femoral arteries because of extensive calcifications, MPCPR clearly excludes stenosis of the aorta and demonstrates the extent of stenosis and occlusions in the femoral arteries (magnified views), which are confirmed with corresponding DSA images. Collateral vessels are not reliably seen with MPCPRs.

(Appendix E1 [<http://radiology.rsna.org/cgi/content/full/2441060976/DC1>]).

MIP Images

A set of 21 MIP images was generated at viewing angles that were identical to those at which the MPCPR images were generated from each of the 10 data sets. A semiautomated bone-editing algorithm (18) was employed by the same radiologist who processed the CT images to suppress bone structures. MIP images were again batch-generated automatically and saved in DICOM format.

Quantification of the Angular Visibility Range by Using MPCPRs Compared with MIPs

To quantify the viewing angle-dependent visibility of peripheral arterial tree

segments (angular visibility range), we conducted the following experiment. Three radiologists (A. Koechl, A.N., and J.E.R., with 2, 3, and 5 years of clinical experience in CT angiography, respectively) independently assessed the visibility of arterial segments for each viewing angle on MPCPR images of all 10 clinical data sets. Images were reviewed in DICOM format at a 1600 × 1200-pixel monitor by using a standard computer workstation (2-GHz dual processor with 2 GB of RAM). The readers could adjust the viewing window settings and could pan, zoom, and rotate the images back and forth over a 180° range in 9° intervals.

For each angular view, 17 arterial segments of the lower extremity arterial tree (Fig 2) were assigned scores with respect to their visibility (score 1, completely visible [the entire vessel is visible]; score 0.5, partially visible [less than 50% of the vessel is obscured by the overlying vessel]; and score 0, not visible [more than 50% of the vessel is obscured by the overlying vessel]). The 17 segments included the following: aorta, CIA, EIA together with CFA, SFA together with popliteal artery, proximal ATA (above the level of the TPT bifurcation), distal ATA, TPT, peroneal artery, and posterior tibial artery. A final visibility score was derived for each segment and each viewing angle by two radiologists (J.E.R. and D.F.) in consensus.

All arterial segments were also assessed on the corresponding MIP images with the same scoring system by two radiologists (J.E.R. and D.F.), who were blinded to the results of the assessment on MPCPRs, in consensus. To reduce any recall bias, the analysis was performed 8 weeks after the assessment with the MPCPRs. In addition, MIP images served for the assessments in regard to the presence of vessel wall calcifications. For each arterial segment, the following classifications were applied: no calcification, spotlike calcifications, plaquelike calcifications (calcifications of less than 50% of the vessel circumference), and circumferential calcifications (calcifications of the vessel circumference or more than 50% of it).

In cases of multiple calcifications per segment, the calcification with the largest circumferential extent was recorded.

Quantification of Orthogonal Viewing Pairs by Using MPCPRs

A pair of two orthogonal curved planar reformation images, such as those obtained in the coronal and sagittal planes, are generally recommended to account for eccentric disease (11,12,14). We were interested in finding out whether such orthogonal viewing pairs could be provided by using MPCPRs. Therefore, the number of fully visible orthogonal viewing pairs for each segment on MPCPRs was counted (J.E.R.). A classification of “completely visible” was defined as that in which both images of a pair had a final visibility score of 1 (100%). The maximum possible number of orthogonal viewing pairs per segment was 11; however, the first pair with -90° and 0° viewing angles and the last pair with 0° and $+90^\circ$ viewing angles were considered redundant.

Conditions That Caused Artifacts on MPCPRs: Synthetic Data

The geometric properties of curved planar reformation image generation aid in the prediction of viewing angle-dependent artifacts when a vessel centerline approaches a course parallel to the transverse (x-y) plane (15); such a situation may occur in the iliac territory and at the origin of the ATA. When the viewing angle is perpendicular to the vessel axis, curved planar reformation may cause spurious dilatation (“positive vessel distortion”) or even doubling (“looping”) of a vessel segment (15).

To explore the particular conditions that cause positive vessel distortion artifacts in MPCPRs with controlled conditions, we generated 12 synthetic aortoiliac CT angiographic data sets that simulated various tilt angles of the external iliac arteries relative to the transverse plane (defined as 0°). The tilt angles ranged from -15° to $+40^\circ$ (negative tilt angles indicate an upward slope relative to the transverse plane). The synthetic data sets were generated in DICOM format by one radiologist (J.E.R.), together with a graduate stu-

Figure 2

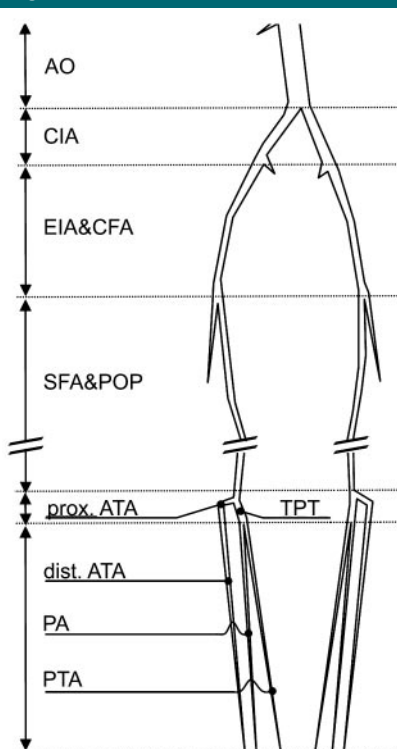


Figure 2: Schematic of vascular segments ($n = 17$) of arteries of the lower extremity. AO = aorta, CIA = common iliac artery, EIA = external iliac artery, CFA = common femoral artery, SFA = superficial femoral artery, POP = popliteal artery (femoropopliteal artery), prox. ATA = proximal ATA, TPT = tibiofibular trunk, dist. ATA = distal ATA. Remaining keys are the same as for Figure 1.

dent (T.R.), by using commercial mathematic software (MatLab; Matworks, Natick, Mass). The vessels were modeled as curved cylindrical objects, with their medial axes as three-dimensional splines, by using six control points. The angles of the tangent of the spline that represented the EIA were obtained by varying the position of one of the control points. MPCPR images and MIP images were again generated for 21 viewing angles and printed side by side in a grid so that rows of images reflect increasing tilt angles and columns of images reflect varying viewing angles. This display allowed the simultaneous visualization of the effect of viewing angles and tilt angles on MPCPR images compared with MIP images.

Conditions That Caused Artifacts on MPCPRs: Clinical Data Sets

All clinical data sets were reviewed by two radiologists (D.F. and J.E.R.) in consensus to specifically identify and count positive vessel distortion artifacts. Artifacts were classified as no artifact (normal vessel appearance), minor artifact (any apparent vessel dilatation that was less than half of the normal vessel lumen), and major artifact (substantial vessel dilatation of more than approximately half of the normal vessel lumen). Iliac and proximal ATA tilt angles were recorded. The readers also were encouraged to identify and describe any other unexpected artifact that they might have observed. To differentiate between artifacts and true vessel distortions, the radiologists used all available images obtained in each patient; these images included transverse images, SPCPRs, MIPs, and DSA images.

Statistical Analysis

Interobserver agreement for arterial visibility scores in MPCPR images was calculated by using a κ statistic (≤ 0.20 , poor; 0.21–0.40, fair; 0.41–0.60, moderate; 0.61–0.80, substantial; 0.81–1.00, excellent) (19). Because the response variable had only three ordinal values of visibility scores, and the distribution of those values was highly skewed (70% = score 1), the response variable with the score of 0.5 was recoded as a score of 0, and a complementary log-log regression

Figure 3

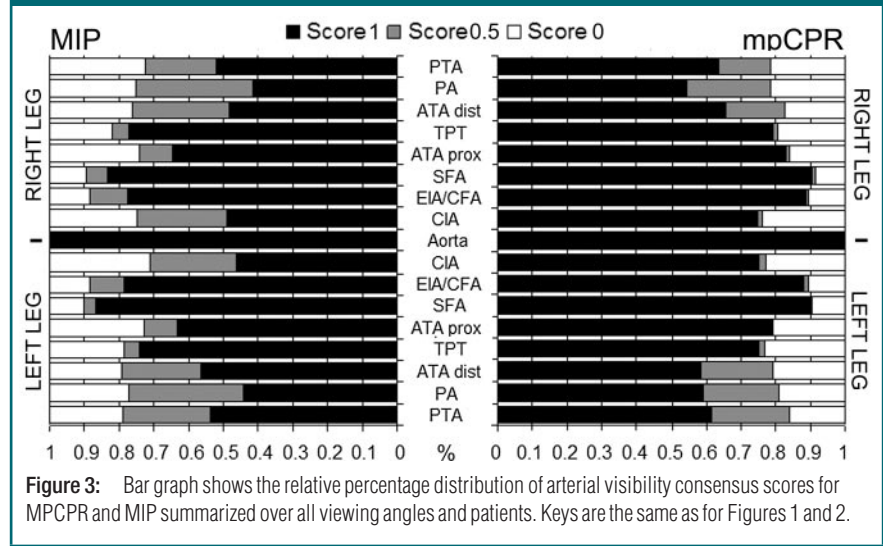


Figure 3: Bar graph shows the relative percentage distribution of arterial visibility consensus scores for MPCPR and MIP summarized over all viewing angles and patients. Keys are the same as for Figures 1 and 2.

was performed with four predictors and their interactions as follows: arterial segment (omitting aorta), side (left and right), viewing angle (from 0° to 180°), and image method (MIP and MPCPR). This yielded odds ratios (ORs) for the relative odds of a rating of 1.

To account for the repeated measurements in patients, a random-effects generalized estimating equation estimation method with an exchangeable correlation structure was used, with patient as the cluster variable. The segment that consists of the EIA and the CFA was considered as the baseline for comparisons among locations. A power analysis suggested that the experiment would aid in the detection of differences in response proportions between MPCPRs and MIPs of 0.10 or larger with 80% power at a 5% error rate. Analysis was performed with software (Stata, version 9.1; Stata, College Station, Tex). A difference with a P value of .05 was considered significant.

Results

Quantification of the Angular Visibility Range by Using MPCPRs Compared with MIPs

Five of 170 arterial segments were occluded and, thus, were excluded from the analysis. For the remaining 165 segments, there was substantial agreement

between the readers in regard to the determination of arterial visibility by using MPCPRs for all vascular segments (readers 1 and 2, $\kappa = 0.67$; readers 1 and 3, $\kappa = 0.63$; and readers 2 and 3, $\kappa = 0.65$).

In general, arterial visibility was greater for MPCPRs than it was for MIPs and was decreased for vessel segments farther down the vascular tree. The specific percentages of a visibility score of 1 per anatomic segment (pooled for left and right leg) for MPCPRs versus MIPs, respectively, was as follows: for the aorta, 100% (210 of 210) versus 100% (210 of 210); for the CIA, 75% (315 of 420) versus 48% (200 of 420); for the EIA and CFA, 88% (371 of 420) versus 78% (328 of 420); for the femoropopliteal artery, 90% (342 of 378) versus 85% (321 of 378); for the proximal ATA, 81% (323 of 399) versus 64% (255 of 399); for the TPT, 77% (324 of 420) versus 76% (318 of 420); for the distal ATA, 62% (234 of 378) versus 52% (198 of 378); for the peroneal artery, 57% (238 of 420) versus 43% (180 of 420); and for the posterior tibial arteries, 62% (262 of 420) versus 53% (222 of 420) (Fig 3). Windmill plots (Fig 4) illustrate the angular distribution of the arterial visibility for MPCPRs and MIPs. Angular viewing ranges were maximal at the level of the aorta and smallest at the level of the crural arteries below the TPT bifurcation.

The results of the multiple regression analysis showed a significant main

effect of image method (OR for MPCPR or MIP = 1.55, $P < .001$), with an overall increase in the probability of a response of completely visible of about 10% with MPCPR compared with MIP. There was also a significant effect of

arterial segment: All ORs except those for the CIA and for the SFA and popliteal artery were less than 1.00 relative to the EIA and the CFA ($P < .001$). There was an additional interaction between the effects of image method and arterial segment for the CIA (OR = 1.54, $P < .001$), and this interaction caused an increase in the OR between MPCPR and MIP to 2.40 in that segment. There was no significant overall effect of viewing angle (OR = 1.01, $P < .24$), but there was a significant interaction between viewing angle and arterial segment for the CIA relative to the EIA and the CFA (OR = 1.04, $P < .001$). There was no significant effect of side (left or right) (OR = 1.00, $P < .93$). The estimated within-subject correlation was 0.004.

Of all 165 vascular segments analyzed in 10 patients, only 32% (53 of 165) had no calcifications on MIP images. Spotlike calcifications were seen in 22% (36 of 165) of vessel segments, plaque-like calcifications were seen in 13% (22 of 165) of vessel segments, and circumferential calcifications with complete obscuration of the lumen were seen in 33% (54 of 165) of vessel segments. Circumferentially calcified segments were found in all 10 patients, with a mean of five segments (range, 1–11) per patient.

Quantification of Orthogonal Viewing Pairs by Using MPCPR

In all 10 patients, at least one or more fully visible orthogonal viewing pairs existed for all vascular segments proximal to the level of the TPT bifurcation (Fig 5). However, complete orthogonal viewing pairs were not always present in the arterial segments below the level of the TPT, where six paths (bilateral anterior and posterior tibial and peroneal arteries) contribute to an MPCPR image.

Conditions That Cause Artifacts on MPCPRs: Synthetic Data

We were able to reproduce vessel distortion artifacts in MPCPR images of the synthetic aortoiliac phantom in situations in which small or negative tilt angles (ie, vessel axis approaching or coursing upward relative to the trans-

verse plane) concurred with lateral viewing angles relative to the iliac arteries (Fig 6). However, there was a wide range of viewing angles (from -54° to $+54^\circ$) that were free of major artifacts, for tilt angles are greater than -10° . No artifacts were seen from any viewing angle for tilt angles greater than $+15^\circ$.

Conditions That Cause Artifacts on MPCPRs: Clinical Data Sets

Major vessel distortion artifacts were present in only three patients at the level of the ATA; minor artifacts occurred in two patients at the level of the EIA and in one patient at the level of the ATA (Table). In three patients, we found pseudostenoses caused by inaccurate centerline placement. We also observed two other types of MPCPR-specific artifacts in all of our patients. Crossing artifacts occurred in those views in which centerline paths were crossing each other and resulted in characteristic horizontal bands of discontinuities in the MPCPR image. Because of the characteristic appearance and the specific circumstances of occurrence and because minimal rotation (eg, 9°) eliminates or relocates this phenomenon, it is easily identified as an artifact (Fig 7). Finally, we found subtle suture artifacts—abrupt oblique vertically oriented transitions exactly halfway between arterial paths—where the curved reconstruction planes abut each other in all patients (Fig 7).

Discussion

Our findings confirm that three-dimensional visualization alone is inadequate for interpreting CT angiograms of the peripheral arteries in patients with PAOD (1–8,10–12,14,20,21). We found circumferential vessel calcifications that completely obscured the flow lumen of arterial segments in MIP images in all of our 10 patients. Cross-sectional analysis of arteries obscured by calcifications or stents is very time consuming when it is performed by using transverse source image viewing, and even standard SCPRs are not truly comprehensive.

The possibility of simultaneously displaying longitudinal cross sections

Figure 4

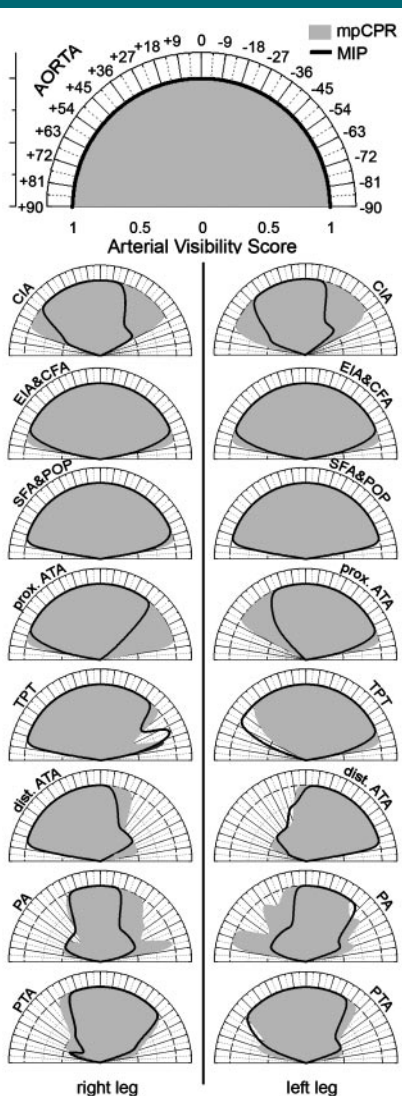


Figure 4: Windmill plots show the angular visibility range for vascular segments in MPCPRs and MIPs. Radial axis represents the visibility score of 1, 0.5, or 0; viewing angles range from $+90^\circ$ (right lateral view) to -90° (left lateral view). Note that the lateral views have the worst visibility for all segments except the aorta. Visibility of crural arteries is limited to comparably small unobstructed angular viewing ranges. Keys are the same as for Figures 1 and 2.

Figure 5

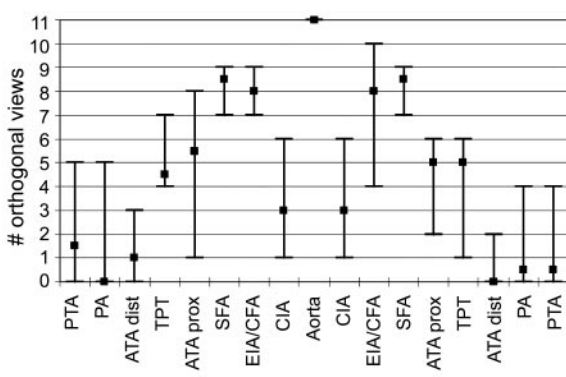


Figure 5: Graph shows median (quadrates) and full range (whiskers) of the number of fully visible orthogonal viewing pairs for each vascular segment in all 10 patients. A classification of completely visible is defined as a visibility score of 1 for both perpendicular views. At least one or more orthogonal viewing pairs existed for all vascular segments above the TPT—with the maximum of 11 orthogonal viewing pairs at the level of the aorta—whereas more distally this was not always the case with patients in whom there were no orthogonal viewing pairs. Keys are the same as for Figure 3.

through all the major conducting arteries of a diseased peripheral arterial tree by using MPCPRs is, thus, a very attractive potential solution to an important practical limitation of CT angiography of the peripheral arteries. Because the therapeutically relevant morphologic information sought in patients with peripheral vascular disease lies almost exclusively in the conducting arteries, MPCPRs might not only rival standard SPCPRs but also challenge current three-dimensional visualization techniques, such as MIP and volume rendering. To further evaluate MPCPR, we examined its display properties and its limitations compared with the performance of MIP and that of SPCPR; MIP and SPCPR are routinely used in this setting.

Because MPCPR displays several vessels on an image, the apparent concern is that these vessels may overlap and, thus, can obscure each other from certain viewing angles. Our quantitative assessment of arterial visibility indeed demonstrated vessel overlap, which was viewing angle dependent and more pronounced farther down the arterial tree where an increasing number of centerline paths contribute to the computed image. However, arterial visibility of MPCPR was slightly (10%) but significantly greater than that of MIP. This finding is explained by the spatial arrangement of centerlines and by the smaller number of vessels displayed on an MPCPR image compared with an MIP image.

It is generally accepted that at least two orthogonal views—such as coronal

Figure 6

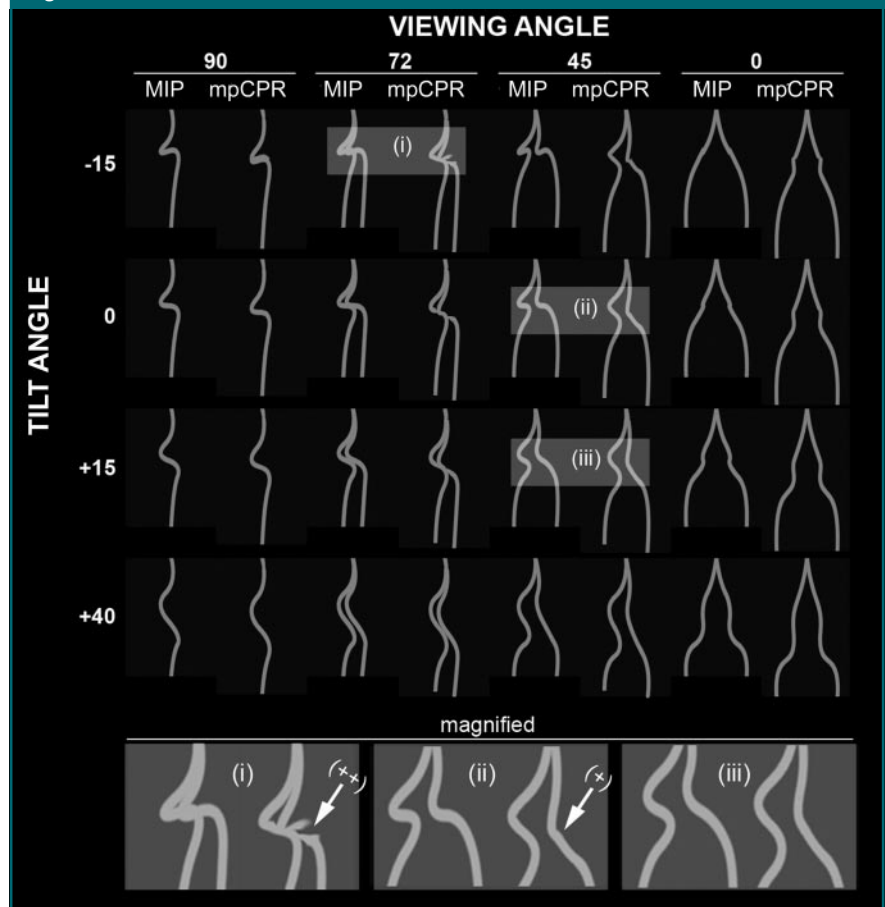


Figure 6: Top: Side-by-side comparison of selected pairs of MIP and MPCPR images obtained with synthetic aortoiliac phantoms. Pairs are grouped in a grid of four columns of viewing angles and four rows of tilt angles. Bottom: Magnified images (i)–(iii) show major (++) and minor (+) positive distortion artifacts (spurious dilatation of the vessel lumen [arrow]), which are also highlighted in top image. Note that the major artifact in image (i) produces a virtual doubling of the vessel lumen, a so-called looping artifact. The severity of artifacts depends on both vessel tilt and viewing angles and is most severe in lateral views of vessels with small or negative tilt angles.

and sagittal—are computed for curved planar reformation display to account for eccentric disease (11–14). If MPCPR provides complete pairs of all vessel segments, one might argue that standard SPCPRs do not need to be generated at all. Our results show, however, that, with the current implementation, one can provide complete curved planar reformation viewing pairs of aorta-to-popliteal artery segments only and that complete viewing pairs cannot be expected for all below-knee segments. This is not surprising because six separate centerline paths contribute to the image formation in this region. Reconstructing MPCPRs through each leg separately (each resulting in only three paths below the knee) would alleviate this problem, but this resolution would be at the cost of decreased overall spatial perception. Therefore, and also because of artifacts that may occur in this particular region, we think that MPCPRs should be combined with a limited set of standard SPCPRs.

As expected, we observed positive vessel distortion artifacts on MPCPRs when the vessel axis approached the transverse plane. Severe distortions were observed at the takeoff of the ATA. Iliac artifacts were only mild in our 10 clinical cases. More severe vessel distortions and the typical looping artifact are expected in cases with more tortuous iliac arteries. The observed pseudostenosis caused by inaccurate centering of a vessel centerline is a general inherent limitation of all curved planar reformations (15,21,22) and not specific to MPCPRs.

Artifacts specific to MPCPRs occur at the sutures where contributing image planes meet in the composite MPCPR image; on a composite MPCPR image, vessel bifurcations of small-diameter branches particularly may cause problems. Although many of these artifacts lead to an unusual appearance of vessels and adjacent structures, they are easily recognized and prompt the observer to rotate the data set. Because all of the

SPCPR and MPCPR artifacts are viewing angle dependent, the ambiguity between artifactual and real stenoses can usually be resolved. Given that this resolution of ambiguity cannot be guaranteed with certainty in all cases, it is helpful to have alternative images, such as MIPs and SPCPRs, in addition to MPCPRs available.

Our study had several limitations. First, it includes only a limited number of subjects with PAOD, and our analysis was limited to the quantification of the arterial visibility and the characterization of artifacts in MPCPR images. We did not address how MPCPR affects accuracy in the detection of atherosclerotic changes and whether use of MPCPR images affects the speed of image interpretation. A rigorous analysis of the work flow with specific assessment of user interaction and processing times is part of an ongoing investigation. Another limitation may be that clinical CT angiographic data sets were acquired with a four-channel multi-detec-

Vascular Tilt Angles and MPCPR Vessel Distortion Artifacts in 10 Patients with PAOD

Patient No./ Age (y)	EIA				ATA				Other Artifacts		
	Tilt Angle (degrees)		MPCPR Distortion		Tilt Angle (degrees)		MPCPR Distortion		Suture	Crossing	Pseudostenosis
	Left	Right	Left	Right	Left	Right	Left	Right			
1/77	14	9	Minor artifact	Minor artifact	34	31	No artifact	No artifact	Present	Present	Absent
2/54	32	20	No artifact	No artifact	45	NA	No artifact	NA	Present	Present	Present
3/76	45	43	No artifact	No artifact	16	41	Minor artifact	No artifact	Present	Present	Absent
4/77	49	53	No artifact	No artifact	38	42	No artifact	No artifact	Present	Present	Absent
5/59	70	64	No artifact	No artifact	11	7	Major artifact	Major artifact	Present	Present	Absent
6/67	51	25	No artifact	No artifact	3	6	Major artifact	Major artifact	Present	Present	Present
7/67	12	9	Minor artifact	Minor artifact	40	40	No artifact	No artifact	Present	Present	Absent
8/78	72	68	No artifact	No artifact	18	49	No artifact	No artifact	Present	Present	Present
9/80	50	48	No artifact	No artifact	8	27	Major artifact	Major artifact	Present	Present	Absent
10/58	60	62	No artifact	No artifact	31	45	No artifact	No artifact	Present	Present	Absent

Note.—NA = not applicable.

tor row CT scanner with lower resolution (3-mm effective section thickness) than our current 16- or 64-channel systems (2-mm effective section thickness). Because the spatial resolution of the data sets affects both MIPs and MPCPRs and because we were predominantly interested in the general MPCPR display properties and not in the accuracy of lesion detection, we believe that this focus does not lessen the validity of our results.

So, is MPCPR the solution to effective visualization in CT angiography of the peripheral arteries? On the basis of our findings, the answer is yes and no. Yes, MPCPR is the most comprehensive technique to visualize the arterial tree in the lower extremity in patients with PAOD. MPCPR allows complete cross-sectional display of the aortoiliac and femoropopliteal arterial segments over a wide viewing range and provides complete orthogonal viewing pairs for all of these segments. Given that aortoiliac inflow disease and femoropopliteal lesions are by far more relevant from a treatment perspective than are crural arteries (23) and that these segments are notoriously obscured by calcifications in MIPs, representing a substantial practical advantage for MPCPR. Percutaneous interventional treatment planning is also facilitated with visualization of the bilateral aortoiliac and femoropopliteal territories on a single image. The answer is no, however, to the question of whether MPCPR can completely replace MIP and SPCPR. MIP still provides a better angiographic-like overview that includes collateral vessels. If complete cross-sectional evaluation of all crural arteries is therapeutically relevant, SPCPRs are necessary, and SPCPRs also have fewer artifacts.

A practical strategy for the interpretation of CT angiograms of the peripheral arteries might be to provide the reader with several sets of images to choose from. A reader may obtain a quick overview by inspecting the MIP images first. If obscuring calcifications or stents are present, which occurs in the majority of patients with PAOD, he or she may interrogate the MPCPR images next, possibly side by side with the

Figure 7

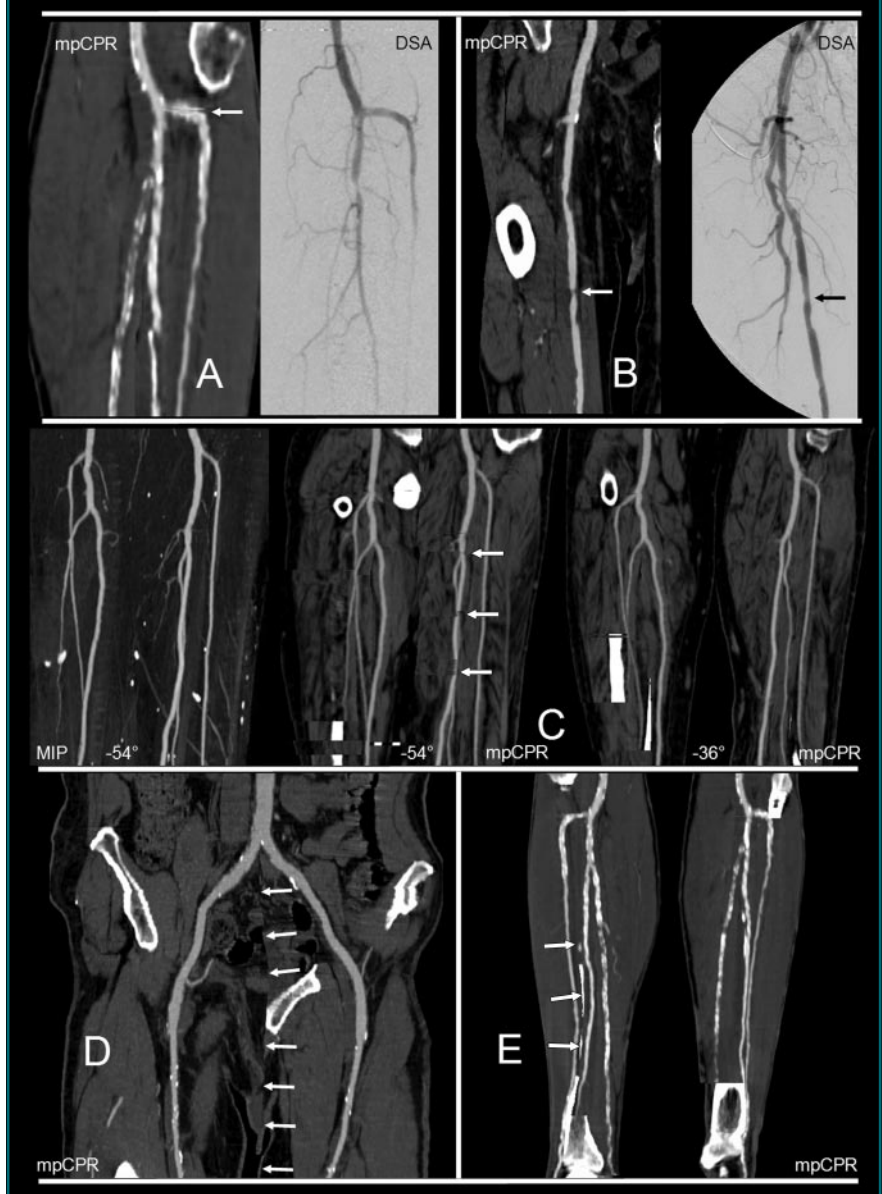


Figure 7: *A*, MPCPR shows horizontal course of the proximal ATA that causes a major positive vessel distortion artifact (spurious vessel dilatation [arrow]). Corresponding DSA image shows normal vessel diameter. *B*, MPCPR image shows spurious narrowing (arrow) of the right SFA. The artifact was due to suboptimal centerline extraction in this location. Corresponding DSA image shows location with subtle stenosis (arrow). *C*, Views show crossing artifacts that occur where centerlines cross each other; included is a view of crural arteries at -54° where the peroneal and posterior tibial arteries cross each other three times (arrows). Crossing artifacts are resolved by rotating the data set to -36° . Corresponding MIP shows no artifact in the overlying vessels. (*D*, *E*) MPCPRs show subtle suture artifacts halfway between arterial paths (arrows), *D*, at the level of the iliac arteries and *E*, at the level of the tibial arteries, with the latter containing a small chip of the tibial bone (arrows).

MIPs. Only in the event that MPCPRs do not allow complete cross-sectional evaluation of all clinically relevant segments, additional SPCPRs, or even transverse images, may be analyzed. Overall, we conclude that MPCPR provides the most comprehensive cross-sectional visualization for CT angiography of the peripheral arteries, but it cannot completely replace MIP and SPCPR.

Acknowledgments: The authors thank Jarrett Rosenberg, PhD, and David N. Tran, BSEE, both of whom are from Department of Radiology, Stanford University Medical Center, Stanford, Calif, for statistical assistance and text and figure editing, respectively.

References

1. Kock MC, Adriaensens ME, Pattynama PM, et al. DSA versus multi-detector row CT angiography in peripheral arterial disease: randomized controlled trial. *Radiology* 2005; 237:727–737.
2. Ouwendijk R, de Vries M, Pattynama PM, et al. Imaging peripheral arterial disease: a randomized controlled trial comparing contrast-enhanced MR angiography and multi-detector row CT angiography. *Radiology* 2005; 236:1094–1103.
3. Willmann JK, Baumert B, Schertler T, et al. Aortoiliac and lower extremity arteries assessed with 16-detector row CT angiography: prospective comparison with digital subtraction angiography. *Radiology* 2005;236:1083–1093.
4. Fleischmann D, Hallett RL, Rubin GD. Computed tomographic angiography of peripheral arterial disease. *J Vasc Interv Radiol* 2006;17:3–26.
5. Catalano C, Fraioli F, Laghi A, et al. Infrarenal aortic and lower-extremity arterial disease: diagnostic performance of multi-detector row CT angiography. *Radiology* 2004; 231:555–563.
6. Edwards AJ, Wells IP, Roobottom CA. Multidetector row CT angiography of the lower limb arteries: a prospective comparison of volume-rendered techniques and intra-arterial digital subtraction angiography. *Clin Radiol* 2005;60:85–95.
7. Martin ML, Tay KH, Flak B, et al. Multidetector CT angiography of the aortoiliac system and lower extremities: a prospective comparison with digital subtraction angiography. *AJR Am J Roentgenol* 2003;180: 1085–1091.
8. Ofer A, Nitecki SS, Linn S, et al. Multidetector CT angiography of peripheral vascular disease: a prospective comparison with intraarterial digital subtraction angiography. *AJR Am J Roentgenol* 2003;180:719–724.
9. Portugaller HR, Schoellnast H, Hausegger KA, Tiesenhäuser K, Amann W, Berghold A. Multislice spiral CT angiography in peripheral arterial occlusive disease: a valuable tool in detecting significant arterial lumen narrowing? *Eur Radiol* 2004;14:1681–1687.
10. Ota H, Takase K, Igarashi K, et al. MDCT compared with digital subtraction angiography for assessment of lower extremity arterial occlusive disease: importance of reviewing cross-sectional images. *AJR Am J Roentgenol* 2004;182:201–209.
11. Prokesch RW, Coulam CH, Chow LC, Bammer R, Rubin GD. CT angiography of the subclavian artery: utility of curved planar reformations. *J Comput Assist Tomogr* 2002;26:199–201.
12. Rubin GD, Schmidt AJ, Logan LJ, Sofilos MC. Multi-detector row CT angiography of lower extremity arterial inflow and runoff: initial experience. *Radiology* 2001;221:146–158.
13. Achenbach S, Moshage W, Ropers D, Bachmann K. Curved multiplanar reconstructions for the evaluation of contrast-enhanced electron beam CT of the coronary arteries. *AJR Am J Roentgenol* 1998;170:895–899.
14. Raman R, Napel S, Beaulieu CF, Bain ES, Jeffrey RB Jr, Rubin GD. Automated generation of curved planar reformations from volume data: method and evaluation. *Radiology* 2002;223:275–280.
15. Kanitsar A, Fleischmann D, Wegenkittl R, Felkel P, Groeller E. CPR: curved planar reformation. In: *IEEE visualization*. Boston, Mass: IEEE Computer Society, 2002; 37–44.
16. Sramek M, Dimitrov LI. f3d: a file format and tools for storage and manipulation of volumetric data sets. In: *Proceedings of the First International Symposium on 3D Data Processing, Visualization and Transmission*, Padova, Italy, June 19–21, 2002. Los Alamitos, Calif: IEEE Computer Society, 2002; 368–372.
17. La Cruz A, Straka M, Koechl A, Sramek M, Groeller E, Fleischmann D. Non-linear model fitting to parameterize diseased blood vessels. In: *IEEE visualization*. Austin, Tex: IEEE Computer Society, 2004; 393–400.
18. Kanitsar A, Wegenkittl R, Felkel P, Fleischmann D, Sandner D, Groeller E. Computed tomography angiography: a case study of peripheral vessel investigation. In: *IEEE visualization*. San Diego, Calif: IEEE Computer Society, 2001; 477–480.
19. Landis JR, Koch GG. An application of hierarchical kappa-type statistics in the assessment of majority agreement among multiple observers. *Biometrics* 1977;33:363–374.
20. Adriaensens ME, Kock MC, Stijnen T, et al. Peripheral arterial disease: therapeutic confidence of CT versus digital subtraction angiography and effects on additional imaging recommendations. *Radiology* 2004;233: 385–391.
21. Portugaller HR, Schoellnast H, Tauss J, Tiesenhäuser K, Hausegger KA. Semitransparent volume-rendering CT angiography for lesion display in aortoiliac arteriosclerotic disease. *J Vasc Interv Radiol* 2003;14:1023–1030.
22. La Cruz A. Accuracy evaluation of different centerline approximations of blood vessels. In: Deussen O, Hansen C, Keim D, Saube D, eds. *Data visualization 2004: proceedings of the VisSym '04—Sixth Joint Visualization Symposium of the Eurographics Association and the IEEE Computer Society Technical Committee on Visualization and Graphics*, May 19–21, 2004, Konstanz, Germany. Wellesley, Mass: Peters, 2004; 1–11.
23. Ouriel K. Peripheral arterial disease. *Lancet* 2001;358:1257–1264.

Radiology 2007

This is your reprint order form or pro forma invoice

(Please keep a copy of this document for your records.)

Reprint order forms and purchase orders or prepayments must be received 72 hours after receipt of form either by mail or by fax at 410-820-9765. It is the policy of Cadmus Reprints to issue one invoice per order.

Please print clearly.

Author Name _____
Title of Article _____
Issue of Journal _____ Reprint # _____ Publication Date _____
Number of Pages _____ KB # _____ Symbol Radiology
Color in Article? Yes / No (Please Circle)

Please include the journal name and reprint number or manuscript number on your purchase order or other correspondence.

Order and Shipping Information

Reprint Costs (Please see page 2 of 2 for reprint costs/fees.)

_____ Number of reprints ordered \$ _____
_____ Number of color reprints ordered \$ _____
_____ Number of covers ordered \$ _____
Subtotal \$ _____
Taxes \$ _____

(Add appropriate sales tax for Virginia, Maryland, Pennsylvania, and the District of Columbia or Canadian GST to the reprints if your order is to be shipped to these locations.)

First address included, add \$32 for
each additional shipping address \$ _____

TOTAL \$ _____

Shipping Address (cannot ship to a P.O. Box) Please Print Clearly

Name _____
Institution _____
Street _____
City _____ State _____ Zip _____
Country _____
Quantity _____ Fax _____
Phone: Day _____ Evening _____
E-mail Address _____

Additional Shipping Address* (cannot ship to a P.O. Box)

Name _____
Institution _____
Street _____
City _____ State _____ Zip _____
Country _____
Quantity _____ Fax _____
Phone: Day _____ Evening _____
E-mail Address _____

* Add \$32 for each additional shipping address

Payment and Credit Card Details

Enclosed: Personal Check _____
Credit Card Payment Details _____

Checks must be paid in U.S. dollars and drawn on a U.S. Bank.

Credit Card: VISA Am. Exp. MasterCard

Card Number _____

Expiration Date _____

Signature: _____

Please send your order form and prepayment made payable to:

Cadmus Reprints

P.O. Box 751903

Charlotte, NC 28275-1903

Note: Do not send express packages to this location, PO Box.

FEIN #: 541274108

Signature _____

Date _____

Signature is required. By signing this form, the author agrees to accept the responsibility for the payment of reprints and/or all charges described in this document.

Invoice or Credit Card Information

Invoice Address Please Print Clearly

Please complete Invoice address as it appears on credit card statement

Name _____
Institution _____
Department _____
Street _____
City _____ State _____ Zip _____
Country _____
Phone _____ Fax _____
E-mail Address _____

Cadmus will process credit cards and Cadmus Journal Services will appear on the credit card statement.

If you don't mail your order form, you may fax it to 410-820-9765 with your credit card information.

Radiology 2007

Black and White Reprint Prices

Domestic (USA only)						
# of Pages	50	100	200	300	400	500
1-4	\$213	\$228	\$260	\$278	\$295	\$313
5-8	\$338	\$373	\$420	\$453	\$495	\$530
9-12	\$450	\$500	\$575	\$635	\$693	\$755
13-16	\$555	\$623	\$728	\$805	\$888	\$965
17-20	\$673	\$753	\$883	\$990	\$1,085	\$1,185
21-24	\$785	\$880	\$1,040	\$1,165	\$1,285	\$1,413
25-28	\$895	\$1,010	\$1,208	\$1,350	\$1,498	\$1,638
29-32	\$1,008	\$1,143	\$1,363	\$1,525	\$1,698	\$1,865
Covers	\$95	\$118	\$218	\$320	\$428	\$530

Color Reprint Prices

Domestic (USA only)						
# of Pages	50	100	200	300	400	500
1-4	\$218	\$233	\$343	\$460	\$579	\$697
5-8	\$343	\$388	\$584	\$825	\$1,069	\$1,311
9-12	\$471	\$503	\$828	\$1,196	\$1,563	\$1,935
13-16	\$601	\$633	\$1,073	\$1,562	\$2,058	\$2,547
17-20	\$738	\$767	\$1,319	\$1,940	\$2,550	\$3,164
21-24	\$872	\$899	\$1,564	\$2,308	\$3,045	\$3,790
25-28	\$1,004	\$1,035	\$1,820	\$2,678	\$3,545	\$4,403
29-32	\$1,140	\$1,173	\$2,063	\$3,048	\$4,040	\$5,028
Covers	\$95	\$118	\$218	\$320	\$428	\$530

International (includes Canada and Mexico)						
# of Pages	50	100	200	300	400	500
1-4	\$263	\$275	\$330	\$385	\$430	\$485
5-8	\$415	\$443	\$555	\$650	\$753	\$850
9-12	\$563	\$608	\$773	\$930	\$1,070	\$1,228
13-16	\$698	\$760	\$988	\$1,185	\$1,388	\$1,585
17-20	\$848	\$925	\$1,203	\$1,463	\$1,705	\$1,950
21-24	\$985	\$1,080	\$1,420	\$1,725	\$2,025	\$2,325
25-28	\$1,135	\$1,248	\$1,640	\$1,990	\$2,350	\$2,698
29-32	\$1,273	\$1,403	\$1,863	\$2,265	\$2,673	\$3,075
Covers	\$148	\$168	\$308	\$463	\$615	\$768

International (includes Canada and Mexico)						
# of Pages	50	100	200	300	400	500
1-4	\$268	\$280	\$412	\$568	\$715	\$871
5-8	\$419	\$457	\$720	\$1,022	\$1,328	\$1,633
9-12	\$583	\$610	\$1,025	\$1,492	\$1,941	\$2,407
13-16	\$742	\$770	\$1,333	\$1,943	\$2,556	\$3,167
17-20	\$913	\$941	\$1,641	\$2,412	\$3,169	\$3,929
21-24	\$1,072	\$1,100	\$1,946	\$2,867	\$3,785	\$4,703
25-28	\$1,246	\$1,274	\$2,254	\$3,318	\$4,398	\$5,463
29-32	\$1,405	\$1,433	\$2,561	\$3,788	\$5,014	\$6,237
Covers	\$148	\$168	\$308	\$463	\$615	\$768

Minimum order is 50 copies. For orders larger than 500 copies, please consult Cadmus Reprints at 800-407-9190.

Reprint Cover

Cover prices are listed above. The cover will include the publication title, article title, and author name in black.

Shipping

Shipping costs are included in the reprint prices. Domestic orders are shipped via UPS Ground service. Foreign orders are shipped via a proof of delivery air service.

Multiple Shipments

Orders can be shipped to more than one location. Please be aware that it will cost \$32 for each additional location.

Delivery

Your order will be shipped within 2 weeks of the journal print date. Allow extra time for delivery.

Tax Due

Residents of Virginia, Maryland, Pennsylvania, and the District of Columbia are required to add the appropriate sales tax to each reprint order. For orders shipped to Canada, please add 7% Canadian GST unless exemption is claimed.

Ordering

Reprint order forms and purchase order or prepayment is required to process your order. Please reference journal name and reprint number or manuscript number on any correspondence. You may use the reverse side of this form as a proforma invoice. Please return your order form and prepayment to:

Cadmus Reprints

P.O. Box 751903
Charlotte, NC 28275-1903

Note: Do not send express packages to this location, PO Box. FEIN #: 541274108

Please direct all inquiries to:

Rose A. Baynard
800-407-9190 (toll free number)
410-819-3966 (direct number)
410-820-9765 (FAX number)
baynardr@cadmus.com (e-mail)

Reprint Order Forms and purchase order or prepayments must be received 72 hours after receipt of form.